 CMES, vol.35, no.1, pp.73-90, 2008

Continuation Schemes for Shape Detection in Inverse Acoustic Scattering Problems

S.-W. Na[1] **and L.F. Kallivokas**[2]

Abstract: We discuss simple numerical schemes, termed continuation schemes, for detecting the location and shape of a scatterer embedded in a host acoustic medium, when considering scant measurements of the scattered acoustic pressure in the vicinity (near- or far-field) of the obstacle. The detection is based on incomplete information, i.e., the measurement stations are distributed in the backscatter region and do not circumscribe the sought scatterer. We consider sound-hard scatterers, and use boundary integral equations for the underlying numerical scheme. We favor amplitude-based misfit functionals, and use frequency- and directionality-continuation schemes to resolve the scatterer's location and shape. We report on numerical experiments that attest to the promise of the schemes.

Keyword: Inverse scattering; shape detection; boundary elements; continuation schemes

1 Introduction

Inverse scattering problems are of considerable practical interest in various areas of science and engineering due, in part, to the ever broadening spectrum of important applications that range from medical (Marin, Power, Bowtell, Sanchez, Becker, Glover, and Jones (2008)), to infrastructure (Wu, Al-Khoury, Kasbergen, Liu, and Scarpas (2007); Tabrez, Mitra, and Gopalakrishnan (2007)), to geophysical, to material (Harris, Mustata, Elliott, Ingham, and Lesnic (2008)) and target identification investigations. In particular, inverse problems arising in acoustics are of relevance in, amongst others, ultrasound imaging (for medical or other non-destructive assessments), seismic imaging, underwater surveillance and target acquisition, and in

[1] Department of Civil, Architectural and Environmental Engineering, The University of Texas at Austin, Austin, TX, USA

[2] Department of Civil, Architectural and Environmental Engineering, The University of Texas at Austin, Austin, TX, USA

the detection of objects in the ocean, either fully submerged or partially buried in the seafloor.

Invariably, in all of the aforementioned areas the common goal is to arrive at a description of unknown characteristics of an interrogated object, whether the characteristics refer to material properties, boundary conditions, geometric measures, etc, by, usually, knowledge of input parameters (e.g. interrogating frequencies), and output measurements (e.g. response at coarsely distributed sensor locations). Due to the incomplete data set such problems are inherently ill-posed (and numerically ill-conditioned), with the ill-posedness originating from any or all of three possible sources, namely, non-existence, non-uniqueness, and/or (numerical) instability (see Colton and Kress (1983, 1998); Kirsch (1996)). To alleviate or overcome the considerable algorithmic challenges imposed by the ill-posedness, specialized schemes, often without sufficient generality, need be devised. In this article, we provide a description of a simple numerical scheme that has, thus far, produced promising results.

Of interest here is the problem of recovering the location and shape of an insonified scatterer from scant measurements of its response when excited by impinging plane waves. In this article, the case of a sound-hard scatterer embedded in full-space is considered. The problem has received considerable attention in the literature, e.g., in Pike and Sabatier (2002); Colton, J., and Monk (2000); and Maponi, Recchioni, and Zirilli (1997).

One may roughly classify the approaches that have been followed, into methods that rely on optimization-based schemes (e.g., Angell, Jiang, and Kleinman (1997); Hass, Rieger, and Lehner (1997); Kress and Zinn (1992); Maponi, Misici, and Zirilli (1991); Misici and Zirilli (1994); Zinn (1989); Kress and Rundell (1994); Kress (1995)), and methods that do not explicitly seek to minimize a misfit functional (e.g., Colton and Kirsch (1996); Colton, Piana, and Potthast (1997); Colton, Giebermann, and Monk (2000); Potthast (1996, 1998)). The latter category is based on the linear sampling method which is originally proposed by Colton and Kirsch Colton and Kirsch (1996). The advantage of the latter category methods is that the shape reconstruction can be carried out without need for *a priori* information, whereas, when optimization methods are used, the feasibility space may be considerably narrowed due to *a priori* knowledge –almost a necessity for robust solution schemes. Typically, in optimization-based schemes the point of departure is the misfit between the measured field response and the field response computed based on assumed shape/location. A considerable body of work exists where solutions are sought based on complete or nearly-complete information: complete information refers to, for example, scattered field data that circumscribe the scatterer, whether in the near- or the far-field.

In this work we favor classical optimization methods for the generality they offer, and focus on a case where information is available only in the backscattered region. Moreover, to deal with the ill-posedness, we combine an amplitude-based misfit functional with a frequency- and (optionally) directionality-continuation algorithm. The continuation scheme implies that a series of inverse problems are solved by iterating over distinct frequencies (and/or directions) of the interrogating waves, while either directly or indirectly taking into account the cumulative effect all frequencies (and/or directions) have on the detection process. The motivation for relying on several frequencies and/or wave incidences for detection (as opposed to, for example, multiple station records circumscribing a scatterer) stems from the fact that, typically, interrogating devices are characterized by frequency/directionality agility, while sensor availability/locations are rather constrained.

2 The forward problem

The typical setup consists of a sound-hard object fully embedded within a homogeneous acoustic host and insonified by traveling plane waves. The associated boundary-value problem, in the frequency domain, is governed by the Helmholtz equation. Let Γ be a closed surface with exterior $\Omega \subset \Re^2$ (Fig. 1). Ω is occupied by a linear, inviscid, and compressible (acoustic) fluid, characterized by wave velocity c. Γ is the bounding surface of a rigid (sound-hard) obstacle S. When S is insonified by an incident wave field u^{inc}, the scattered field can be recovered as the solution to the following problem:

$$\Delta u^s(\boldsymbol{x}) + k^2 u^s(\boldsymbol{x}) = 0, \quad \boldsymbol{x} \in \Omega, \tag{1}$$

$$u^s_\nu(\boldsymbol{x}) = -u^{\text{inc}}_\nu(\boldsymbol{x}), \quad \boldsymbol{x} \in \Gamma, \tag{2}$$

$$\lim_{r\to\infty} \sqrt{r}(u^s_r - iku^s) = 0. \tag{3}$$

In these equations u^s denotes scattered pressure; $\boldsymbol{x}$ is the position vector; $\boldsymbol{\nu}$ is the outward unit normal on Γ (pointing to the interior of S); Δ is the Laplace operator; u^s_ν denotes the normal derivative of the pressure u^s; k denotes wavenumber ($k = \frac{\omega}{c}$, with ω denoting circular frequency). Condition (3), in which r is radial distance and u^s_r the derivative of the pressure along the radial direction, is the Sommerfeld radiation condition. The incident field u^{inc} describes incoming plane waves, i.e.:

$$u^{\text{inc}} = e^{-ik(x\cos\alpha + y\sin\alpha)}, \tag{4}$$

in which α is the angle formed between the normal to the traveling wave front and the x-coordinate axis. With these definitions, and for a smooth boundary Γ,

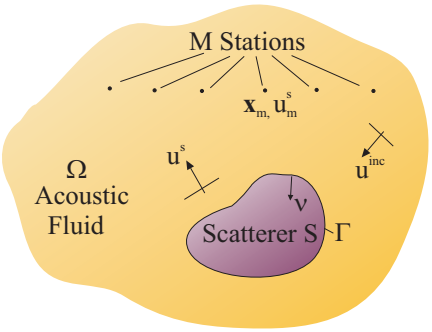

Figure 1: Scattering from a sound-hard object and sampling stations

solutions to Eq. 1-Eq. 3 can be obtained by the following standard integral representations:

$$u^s = \mathfrak{S}[u^s_\nu] - \mathfrak{D}[u^s], \text{ in } \Omega, \tag{5}$$

where $\mathfrak{S}$ and $\mathfrak{D}$ are the single- and double-layers defined for any smooth function q, as[1]:

$$\mathfrak{S}[q](\boldsymbol{x}) = \int_\Gamma q(\boldsymbol{y}) G(\boldsymbol{x},\boldsymbol{y})\, d\Gamma(\boldsymbol{y}), \quad \boldsymbol{x} \in \Omega, \boldsymbol{y} \in \Gamma, \tag{6}$$

$$\mathfrak{D}[q](\boldsymbol{x}) = \int_\Gamma q(\boldsymbol{y}) \frac{\partial G(\boldsymbol{x},\boldsymbol{y})}{\partial \nu_y}\, d\Gamma(\boldsymbol{y}), \quad \boldsymbol{x} \in \Omega, \boldsymbol{y} \in \Gamma, \tag{7}$$

and $G(z)$ in Eq. 6-Eq. 7 is the fundamental solution, i.e.,

$$G(z) = \frac{i}{4} H_0^{(2)}(kz), \tag{8}$$

where $z = |\boldsymbol{x} - \boldsymbol{y}|$ is the distance between a point $\boldsymbol{x}$ within Ω and a point $\boldsymbol{y}$ on Γ; $H_0^{(2)}$ denotes the zeroth order Hankel function of the second kind, and $i = \sqrt{-1}$ is the imaginary unit. Equation (5) provides the scattered field in Ω; by taking into account the following jump relations,

$$\lim_{\Omega \ni \boldsymbol{x} \to \boldsymbol{x} \in \Gamma} \mathfrak{S}[q](\boldsymbol{x}) = S[q](\boldsymbol{x}), \text{ or } \mathfrak{S}[q] = S[q], \tag{9}$$

$$\lim_{\Omega \ni \boldsymbol{x} \to \boldsymbol{x} \in \Gamma} \mathfrak{D}[q](\boldsymbol{x}) = -\frac{1}{2} q(\boldsymbol{x}) + D[q](\boldsymbol{x}), \text{ or } \mathfrak{D}[q] = -\frac{1}{2} q + D[q], \tag{10}$$

[1] Euler script letters (e.g. $\mathfrak{S}$) are used for domain representations of the layers, (i.e., when $\boldsymbol{x} \in \Omega$) and roman letters (e.g. S) for their boundary counterparts (i.e., when $\boldsymbol{x} \in \Gamma$).

in which

$$S[q](\boldsymbol{x}) = \int_{\Gamma} q(\boldsymbol{y}) G(\boldsymbol{x},\boldsymbol{y})\, d\Gamma(\boldsymbol{y}), \quad \boldsymbol{x},\boldsymbol{y} \in \Gamma, \tag{11}$$

$$D[q](\boldsymbol{x}) = \int_{\Gamma} q(\boldsymbol{y}) \frac{\partial G(\boldsymbol{x},\boldsymbol{y})}{\partial \nu_{\boldsymbol{y}}} d\Gamma(\boldsymbol{y}), \quad \boldsymbol{x},\boldsymbol{y} \in \Gamma, \tag{12}$$

it follows that:

$$\frac{1}{2} u^s - S[u^s_\nu] + D[u^s] = 0, \text{ on } \Gamma. \tag{13}$$

Boundary integral equation (13) provides the basis for the numerical solution of the forward problem, for any given instantiation of Γ. As it is well-known, for exterior Helmholtz problems there exists a set of characteristic frequencies for which the integral operators become singular and lead to non-unique solutions. Though mindful of the difficulty, any particular scheme to alleviate this non-uniqueness is not implemented, primarily due to the extremely narrow support of the singular frequencies in the spectrum[2]. In the literature, one can find several remedies for overcoming the singular-frequencies difficulty via specialized schemes, e.g., Burton and Miller (1971), Brakhage and Werner (1965), Bielak, MacCamy, and Zeng (1995). Alternatively, one can resort to a domain decomposition method that automatically alleviates the problem, as was shown in Zeng, Kallivokas, and Bielak (1992).

3 The inverse problem

Next, at a discrete set of M stations (Fig. 1) located in Ω, the scattered pressure field, generated when waves impinge upon the scatterer S, is being sampled. In order to resolve the unknown location and shape of the interrogated scatterer, we seek to minimize, subject to Eq. 1-Eq. 3, appropriately constructed misfit functionals. Natural choices include the misfit defined either by:

$$\mathscr{L}_1(\Gamma) = \frac{1}{2} \sum_{m=1}^{M} \frac{|u^s(\boldsymbol{x}_m) - u^s_m(\boldsymbol{x}_m)|^2}{|u^s_m(\boldsymbol{x}_m)|^2}, \tag{14}$$

or by,

$$\mathscr{L}_2(\Gamma) = \frac{1}{2} \sum_{m=1}^{M} \frac{\left(|u^s(\boldsymbol{x}_m)| - |u^s_m(\boldsymbol{x}_m)|\right)^2}{|u^s_m(\boldsymbol{x}_m)|^2}. \tag{15}$$

[2] For the singularities to manifest in a numerical scheme the frequencies must be prescribed with very fine accuracy (several decimals).

In Eq. 14-Eq. 15, $\boldsymbol{x}_m$ denotes the location of the stations, u^s_m denotes the measured scattered field at the same points, and u^s denotes the forward solution (computed), also at the M locations. Notice, that $\mathscr{L}_1$ defines the misfit in the least-squares sense of the complex-valued scattered field, whereas $\mathscr{L}_2$ defines the misfit between the amplitudes of the same field; both functionals are normalized with respect to the measured field and both are real-valued. We experimented numerically with both of Eq. 14-Eq. 15: whereas Eq. 14 is highly oscillatory for higher frequencies, Eq. 15 presents fewer local minima, and may be preferable, even though it is missing, in an explicit sense, the phase-angle information. Notice that the choice of either Eq. 14 or Eq. 15 is not unique, nor necessarily optimal from a numerical point of view. To implement the minimization of either misfit, irrespective of the optimizer choice, there is need to compute the first- (and possibly higher also) variations of $\mathscr{L}_1$ or $\mathscr{L}_2$ to perturbations of the (unknown) boundary Γ. Numerical differentiation via a finite difference scheme is the simplest choice, and it is what was followed herein. However, finite difference schemes may contribute to, or exacerbate the numerical instability inherent in the inverse problem: a way to elegantly overcome the numerical differentiation associated with the sequence of scatterer boundaries is to adopt a PDE-constrained optimization approach. Accordingly, the misfit functionals are augmented by a weak imposition of the governing PDE, via Lagrange multipliers (e.g. Na and Kallivokas (2008)). Taking the first variations of the augmented functional with respect to the Lagrange multipliers and the primary variable gives rise to state and adjoint problems, respectively. It can then be shown (Bonnet (1995); Na and Kallivokas (2008)) that variations of the functional with respect to boundary perturbations are readily computable, without resorting to a finite difference scheme. Such an approach stands to benefit and be enhanced, numerically, by the simple continuation scheme reported herein. Lastly, as it can be seen from either Eq. 14 or Eq. 15, no term encompassing *a priori* information has been added to the functional. If such information is available, a regularization term can be easily added.

4 Numerics

4.1 Implementation

For the applications considered here, the location and shape of the boundary Γ depends on a small set of parameters. For example, for the case of a circular scatterer, the coordinates of its center and the radius were considered as the unknown parameters (in this case, *a priori* information is implicitly taken into account). Similar assumptions were made for other shapes with which we experimented herein; arbitrary geometries were not considered (i.e. nodal coordinates as

parameters), since a non-self-intersecting algorithm was not implemented. To seek a minimum for the misfit functionals (14) or (15), we used a conjugate-gradient approach (Polak-Ribière); for the computation of the gradient functionals we used finite differences. For each update of the unknown parameters the forward problem needs to be solved: to this end, we implemented boundary integral equation (13) using quadratic isoparametric elements.

Throughout all numerical experiments the stations are located along a fixed y-coordinate (Fig. 1); the motivation stems from practical considerations, for it is rare that sensor distributions circumscribe a scatterer. Furthermore, for all numerical experiments "inverse crimes" are avoided when generating the synthetic data at the measurement stations by either resorting to exact solutions whenever available (e.g. circular scatterer), or to fine boundary parameterizations different than those used for the detection process.

4.2 Numerical Results

To illustrate our preference to $\mathscr{L}_2$ over $\mathscr{L}_1$, we consider first the simple case of a circular scatterer of unit radius ($a = 1$) insonified by a plane wave forming a (-45^o) angle with the x-axis (Fig. 2), where the measurements are taken at the three stations shown in figure 2 (schematic is in scale). We consider the coordinates of the center as the unknown parameters. The forward problem Eq. 13 is solved for the true values $(0,0)$, and for positions of the assumed scatterer anywhere within the dotted square region (Fig. 2). Based on these solutions, we then construct the misfit functionals $\mathscr{L}_1$ and $\mathscr{L}_2$ for all possible positions of the scatterer within, again, the dotted region. Figure 3 depicts the distribution of the misfit functionals for three different interrogating frequencies ($ka = 0.1, 1.0, 5.0$) over the space of feasible values for the scatterer's center's coordinates between -6 and 6 (for both x and y). We remark that the actual inverse problem has one more parameter, the radius; however, we have observed that convergence to the true radius is achieved within the first couple iterations, and thus the graphs shown in Fig. 3 represent cross-sections, for constant radius, of the misfits in four-dimensional space.

Notice the oscillatory nature of $\mathscr{L}_1$ for the higher frequencies that effectively results in multiple minima that are difficult to distinguish from the global minimum (at (0,0)). In fact, it is observed that, as the frequency increases, the basin of attraction of the global minimum narrows considerably when compared with the lower frequencies. As a result, with local optimization schemes, it would be difficult for an optimizer to escape the neighborhood of a local minimum in order to converge to the global one. Mindful of these observations, we favor the use of $\mathscr{L}_2$, and a frequency-continuation scheme for resolving the global minimum. We remark that the behavior depicted in Fig. 3 is similarly encountered in problems characterized

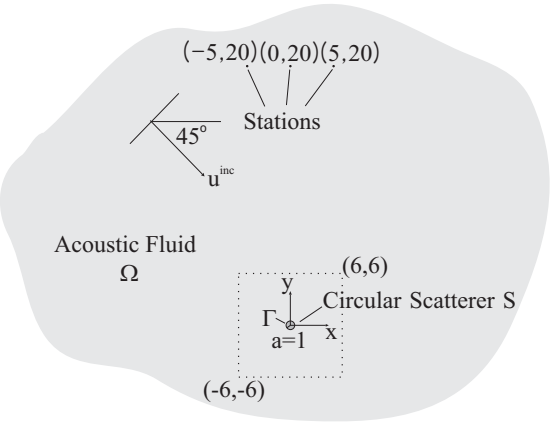

Figure 2: Model problem with a circular scatterer

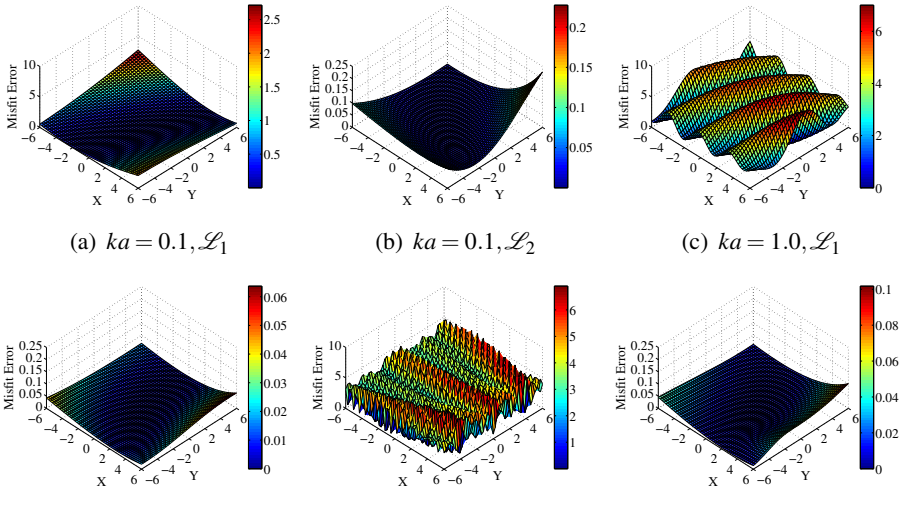

(a) $ka = 0.1, \mathscr{L}_1$ (b) $ka = 0.1, \mathscr{L}_2$ (c) $ka = 1.0, \mathscr{L}_1$

(d) $ka = 1.0, \mathscr{L}_2$ (e) $ka = 5.0, \mathscr{L}_1$ (f) $ka = 5.0, \mathscr{L}_2$

Figure 3: Distribution of misfit functionals $\mathscr{L}_1$ and $\mathscr{L}_2$ for the problem shown in Fig. 2

by a higher dimensionality of the parameter space.

Given a frequency and a set of initial guesses for the unknown parameters, our scheme for a single frequency is encapsulated in the simple algorithm shown below (Algorithm 1).

Algorithm 1 Single-frequency scheme

```
Set ModelParameters
Set Tolerances Tol and MaxIterations
MisfitNorm=1
Iterations = 1
Compute Misfit
while (MisfitNorm < Tol) and (Iterations < MaxIterations) do
    OldMisfit = Misfit
    Compute Gradients
    Compute CG-SearchDirection
    Perform linesearch
    Update ModelParameters
    Compute Misfit
    NewMisfit = Misfit
    MisfitNorm = 2|OldMisfit−Misfit| / (|OldMisfit|+|Misfit|+ε)
    Iterations = Iterations + 1
end while
if Iterations == MaxIterations then
    Failed
else
    Converged
end if
```

However, even if convergence is achieved, there is no guarantee that the converged parameters are the true ones. To improve, we iterate on the frequency (or wavenumber) space, and the converged parameters of the last frequency are used as initial guesses for the next frequency. We typically use two to four frequencies for the problems considered here. Once the highest frequency has resulted in converged parameters, we revisit the misfit for each one of the frequencies we considered earlier, and re-compute the individual frequency misfits using the final parameter values. If the computed values of the new misfits are less than the ones obtained at the ends of the previous convergence cycles, we consider the scheme to have converged. Schematically, this frequency-continuation approach is depicted in Algorithm 2 below.

Note that the misfit functional $\mathscr{L}_2$ defined in Eq. 15 and depicted in Algorithms 1 and 2 can be, if desired, augmented to account for multiple wave incidences for

Algorithm 2 Frequency-continuation scheme

```
Set ModelParameters
for all Frequencies do
    Set ith-Frequency
    Use ModelParameters
    Single-frequency scheme (Algorithm 1)
    (Save ith-Misfit)
    (Save ConvergedModelParameters)
    Set ModelParameters = ConvergedModelParameters
end for
Set FinalModelParameters = ConvergedModelParameters
for all Frequencies do
    Compute Misfit (Use FinalModelParameters)
    if Misfit > ith-Misfit then
        Failed
    end if
end for
Converged
```

each frequency; accordingly, let (for each frequency):

$$\mathscr{L}_2(\Gamma) = \sum_{i=1}^{i=A} \left[\frac{1}{2} \sum_{m=1}^{M} \frac{\left(|u^s(\boldsymbol{x}_m, \alpha_i)| - |u_m^s(\boldsymbol{x}_m, \alpha_i)|\right)^2}{|u_m^s(\boldsymbol{x}_m, \alpha_i)|^2} \right], \tag{16}$$

where α_i denotes the i-th wave incidence and A is the total number of considered wave directions.

Clearly, Algorithm 2, as sketched, is concerned with a series of decoupled inverse problems, that is, one distinct problem for each frequency (even at multiple wave incidence angles), even though the scatterer is the same. The coupling of all these problems, as sketched, is a loose one: it is achieved through the revisiting of the misfit functional values for all frequencies for those values that correspond to the converged set of parameters for the last considered frequency. Alternatively, one could redefine the $\mathscr{L}_2$ functional to allow simultaneous optimization over all of the considered frequencies, as in:

$$\mathscr{L}_2(\Gamma) = \sum_{n=1}^{N} \sum_{i=1}^{i=A} \left[\frac{1}{2} \sum_{m=1}^{M} \frac{\left(|u^s(\boldsymbol{x}_m, \alpha_i, k_n)| - |u_m^s(\boldsymbol{x}_m, \alpha_i, k_n)|\right)^2}{|u_m^s(\boldsymbol{x}_m, \alpha_i, k_n)|^2} \right], \tag{17}$$

where n denotes the n-th interrogating frequency, N is the total number of considered frequencies, and k denotes wavenumber. The process implied by Eq. 17

is considerably more costly: we experimented with Eq. 17 and have found no appreciable difference to the detection process, and thus still favor the simplicity of Eq. 15 or Eq. 16.

We used the continuation scheme to resolve the location and shape of various scatterers and report here on a subset of our results. Figures 4, 5, and 6 depict the obtained results for a circular, an elliptical, and a"potato"-shaped scatterer (with a small portion of its boundary being non-convex). The shape for the latter scatterer was constructed using 7 parameters and truncated trigonometric series in polar coordinates; specifically, the shape is given for $\theta = 0 \ldots 2\pi$ as $r(\theta) = a_0 + a_1 \cos\theta + a_2 \sin\theta + a_3 \cos 2\theta + a_4 \sin 2\theta + a_5 \cos 3\theta + a_6 \sin 3\theta$. Tables 1 and 2 summarize the characteristics of the three problems, including the initial guesses, number of stations, station locations, and wave incidence angles. In all cases, convergence to the true parameters was attained. Figure 4 depicts the convergence pattern to the target using the frequency continuation scheme with three probing frequencies. Notice that the circular scatterer's center coordinates have converged to specific, yet wrong, values at the end of each frequency probing (Fig. 4a), and that without the aid of the continuation scheme, convergence to the target would not have been attained.

Similarly, Fig. 5 depicts the convergence pattern for an elliptical scatterer, when the initial guess is a circular obstacle. Two probing frequencies are used, but, in this case, we also use two probing directions for each frequency, effectively making use of Eq. 16. Notice that, as shown in Fig. 5b, despite the use of two incidence directions, a single frequency would not have been sufficient in recovering the semiaxes. Probing at a higher frequency, using again both incidences, recovers nicely the target. Similar conclusions can be drawn from the more severe test shown in Fig. 6.

Though we have observed sensitivity of the number of iterations to the initial guess, we have not been able to construct a (reasonable) problem for which the continuation scheme would fail. By contrast, if $\mathscr{L}_1$ were to be chosen, the sensitivity of the algorithm to the initial guess increases, even under the continuation scheme, and we have observed failures. In general, we have observed that probing at low frequencies leads the initial shape closer to the target, with probing at higher frequencies being necessary for refining the shape characteristics.

Lastly, all computations were performed on an Intel Xenon workstation: the total CPU time for each problem was 15.5 minutes, 18.5 minutes, and 70 minutes, respectively. Since the finite difference scheme is used to compute the gradient of the misfit functional, the computational time increases proportionally with the number of unknown parameters. However, as mentioned earlier, if an adjoint approach based on a PDE-constrained optimization is employed (e.g., Na and Kallivokas

(2008)), significant computational cost savings can be expected.

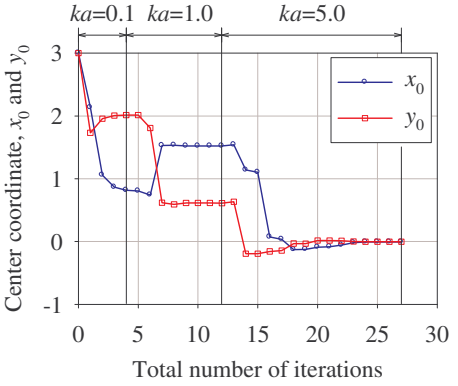

(a) Convergence pattern of the center coordinates

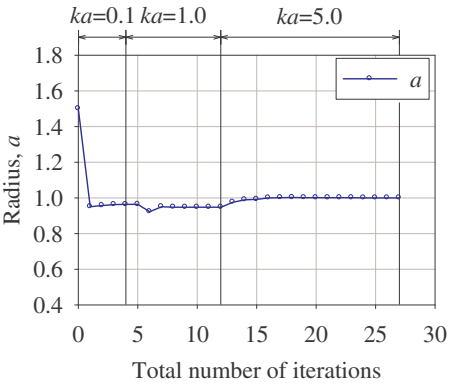

(b) Convergence pattern of the radius

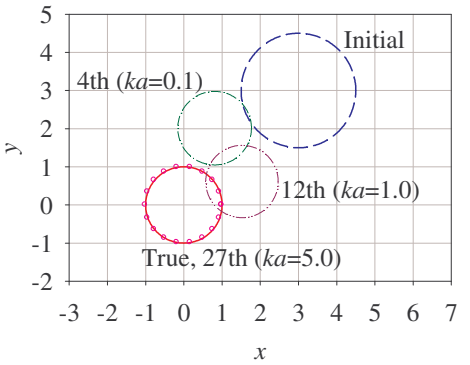

(c) Combined convergence pattern

Figure 4: Inverse problem for a circular scatterer using frequency-continuation

5 Conclusions

We discussed a frequency- and directionality-continuation scheme for resolving the unknown shapes of insonified scatterers, and have applied it to prototype problems involving canonical and arbitrarily-shaped scatterers. The idea is based on feeding the converged estimates of location and shape due to lower frequency probing as initial estimates to the higher probing frequencies. The same approach was used when iterating over wave incidences. We provided an algorithm for ensuring that the final estimates are also checked against all probing frequencies/incidences.

Table 1: Inverse problems characteristics (scatterer shape, parameter definitions, station locations, and incident wave directions)

Scatterer shape	Parameters	Station locations	Waves
Circle	Center and radius (x_0, y_0, a)	(-5,20), (0,20) (5,20)	$\alpha = -45^o$
Ellipse	Center and semi-axes (x_0, y_0, s_M, s_m)	(-10,20), (0,20) (10,20)	$\alpha = -45^o$, 225^o
Potato	Coefficients $(a_0, a_1, \ldots, a_6)$	(-5,20), (0,20) (5,20), (-10,20) (10,20)	$\alpha = -90^o$, 0^o, 180^o

Table 2: Inverse problems parameter values

Scatterer shape	Initial guess	True values	Final values
Circle	(3,3,2)	$x_0 = 0$	-0.0058
	(3,3,2)	$y_0 = 0$	-0.0026
	(3,3,2)	$a = 1$	1.0001
Ellipse	(50,-50,2,2)	$x_0 = 0$	0.0013
		$y_0 = 0$	-0.0011
		$s_M = 1.5$	1.5001
		$s_m = 1$	1.0000)
Potato	(2,0,0,0,	$a_0 = 1$	1.0002
	(2,0,0,0,	$a_1 = 0.2$	0.1977
	(2,0,0,0,	$a_2 = -0.3$	-0.2998
	0,0,0)	$a_3 = 0.125$	0.1246
	0,0,0)	$a_4 = 0.125$	0.1252
	0,0,0)	$a_5 = -0.05$	-0.0504
	0,0,0)	$a_6 = -0.05$	-0.0504

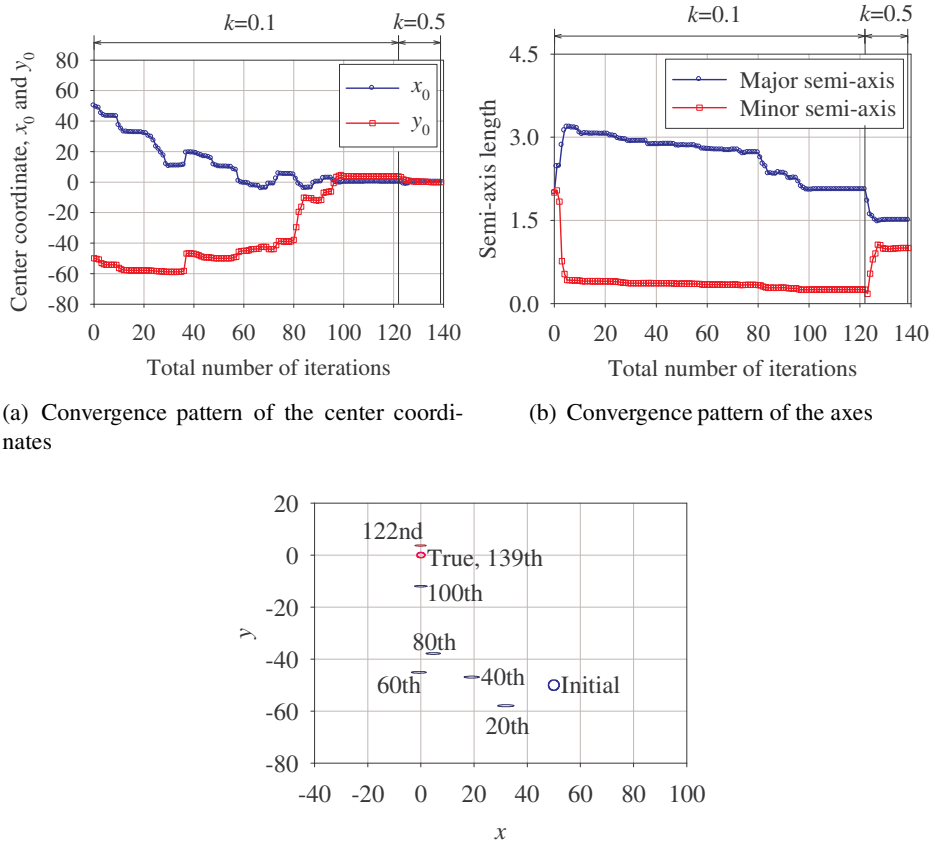

(a) Convergence pattern of the center coordinates

(b) Convergence pattern of the axes

(c) Combined convergence pattern

Figure 5: Inverse problem for an elliptical scatterer using frequency-continuation

Clearly, adding probing frequencies and/or incidences increases the data set (sensor data) used to guide the detection process, and in this sense, solution multiplicity is, somewhat, alleviated. However, augmentation of the data set alone is not necessarily capable of offering algorithmic robustness, since numerical evidence we discussed earlier suggests that reversing the order of the probing, from high to low frequencies, can lead to failure. To date, the combination of amplitude-based misfit functionals, embedded within a frequency-continuation scheme with ascending frequency probing, appears to be robustly recovering scatterer shape and location.

As noted, the underlying numerical scheme is expensive, since it is based on finite differences for the computation of the gradients (derivatives are computed with respect to each shape parameter, requiring, in turn, the solution of Eq. 13 every

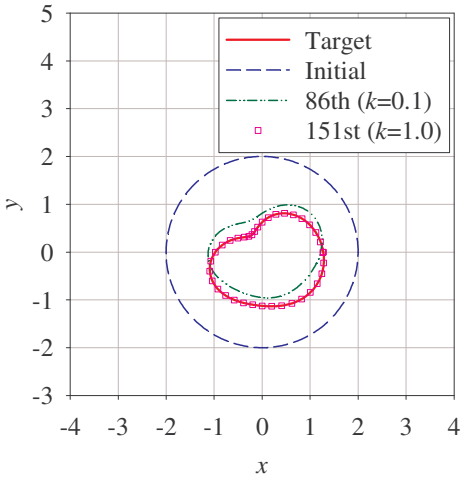

Figure 6: Inverse problem for an arbitrarily-shaped (potato) scatterer using frequency-continuation

single time). However, adjoint formulations can lessen the computational cost, while still retaining the benefits of the proposed continuation schemes.

Acknowledgement: Partial support for the authors' research presented herein has been provided by the National Science Foundation under grant awards CMS-0348484. This support is gratefully acknowledged.

References

Angell, T. S.; Jiang, X.; Kleinman, R. E. (1997): A distributed source method for inverse acoustic scattering. *Inverse Problems*, vol. 13, pp. 531–545.

Bielak, J.; MacCamy, R. C.; Zeng, X. (1995): Stable coupling method for interface scattering problems by combined integral equations and finite elements. *J. Comput. Phys.*, vol. 119, pp. 374–384.

Bonnet, M. (1995): BIE and material differentiation applied to the formulation of obstacle inverse problems. *Engineering Analysis with Boundary Elements*, vol. 15, pp. 121–136.

Brakhage, H.; Werner, P. (1965): Über das Dirichletsche Aussenraumproblem für die Helmoltzsche Schwingungsgleichung. *Arch. Math*, vol. 16, pp. 325–329.

Burton, A. J.; Miller, G. F. (1971): The application of integral equation methods to the numerical solution of some exterior boundary-value problems. *Proc. Royal Soc. London*, vol. 323, pp. 201–210.

Colton, D.; Giebermann, K.; Monk, P. (2000): A regularized sampling method for solving three-dimensional inverse scattering problems. *SIAM Journal on Scientific Computing*, vol. 21, pp. 2316–2330.

Colton, D.; J., J. C.; Monk, P. (2000): Recent developments in inverse scattering theory. *SIAM Review*, vol. 42, pp. 369–414.

Colton, D.; Kirsch, A. (1996): A simple method for solving inverse scattering problems in the resonance region. *Inverse Problems*, vol. 12, pp. 383–393.

Colton, D.; Kress, R. (1983): *Integral Equation Methods in Scattering Theory*. Wiley-Interscience, New York.

Colton, D.; Kress, R. (1998): *Inverse acoustic and electromagnetic scattering theory*. Springer-Verlag, New York.

Colton, D.; Piana, M.; Potthast, R. (1997): A simple method using Morozov's discrepancy principle for solving inverse scattering problems. *Inverse Problems*, vol. 13, pp. 1477–1493.

Harris, S. D.; Mustata, R.; Elliott, L.; Ingham, D. B.; Lesnic, D. (2008): Numerical identification of the hydraulic conductivity of composite anisotropic materials. *CMES: Computer Modeling in Engineering & Sciences*, vol. 25, no. 2, pp. 69–79.

Hass, M.; Rieger, W.; Lehner, G. (1997): Inverse 3D acoustic and electromagnetic obstacle scattering by iterative adaption. *in Inverse Problems in Wave Propagation and Diffraction, G. Chavent and P. Sabatier, eds.*, pp. 204–215.

Kirsch, A. (1996): *An Introduction to the Mathematical Theory of Inverse Problems*. Springer-Verlag, New York.

Kress, R. (1995): Integral equation methods in inverse obstacle scattering. *Engineering Analysis with Boundary Elements*, vol. 15, pp. 171–179.

Kress, R.; Rundell, W. (1994): A quasi-Newton method in inverse obstacle scattering. *Inverse Problems*, vol. 10, pp. 1145–1157.

Kress, R.; Zinn, A. (1992): On the numerical solution of the three dimensional inverse obstacle scattering problem. *Journal of Computational and Applied Mathematics*, vol. 42, pp. 49–61.

Maponi, P.; Misici, L.; Zirilli, F. (1991): An inverse problem for the three dimensional vector Helmholtz equation for a perfectly conduction obstacle. *Journal of Computers & Mathematics with Applications*, vol. 22, pp. 137–146.

Maponi, P.; Recchioni, M.; Zirilli, F. (1997): The use of optimization in the reconstruction of obstacles from acoustic or electromagnetic scattering data. *in Large Scale Optimization with Applications, L. Biegler, et al., eds.*, pp. 81–100.

Marin, L.; Power, H.; Bowtell, R. W.; Sanchez, C. C.; Becker, A. A.; Glover, P.; Jones, A. (2008): Boundary elementmethod for an inverse problem in magnetic resonance imaging gradient coils. *CMES: Computer Modeling in Engineering & Sciences*, vol. 23, no. 3, pp. 149–173.

Misici, L.; Zirilli, F. (1994): Three dimensional inverse obstacle scattering for time harmonic acoustic waves: A numerical method. *SIAM Journal on Scientific Computing*, vol. 15, pp. 1174–1189.

Na, S.-W.; Kallivokas, L. F. (2008): PDE-constrained amplitude-based shape detection in inverse acoustic scattering. *Computational Mechanics*, vol. 41, no. 4, pp. 579–594.

Pike, R.; Sabatier, P. (2002): *Scattering and Inverse Scattering in Pure and Applied Science*. Academic Press, San Diego.

Potthast, R. (1996): A fast new method to solve inverse scattering problems. *Inverse Problems*, vol. 12, pp. 731–742.

Potthast, R. (1998): A point-source method for inverse acoustic and electromagnetic obstacle scattering problems. *IMA Journal of Applied Mathematics*, vol. 61, pp. 119–140.

Tabrez, S.; Mitra, M.; Gopalakrishnan, S. (2007): Modeling of degraded composite beam due to moisture absorption for wave based detection. *CMES: Computer Modeling in Engineering & Sciences*, vol. 22, no. 1, pp. 77–89.

Wu, C.-Y.; Al-Khoury, R.; Kasbergen, C.; Liu, X.-Y.; Scarpas, A. (2007): Spectral element approach for inverse models of 3d layered pavement. *CMES: Computer Modeling in Engineering and Sciences*, vol. 17, no. 3, pp. 163–172.

Zeng, X.; Kallivokas, L. F.; Bielak, J. (1992): Stable localized symmetric integral equation method for acoustic scattering problems. *J. Acoust. Soc. America*, vol. 91, no. 5, pp. 2510–2518.

Zinn, A. (1989): On an optimisation method for the full- and the limited-aperture problem in inverse acoustic scattering for a sound-soft obstacle. *Inverse Problems*, vol. 5, pp. 239–253.